Author Manuscript
Accepted for publication in a peer-reviewed journal

NIST National Institute of Standards and Technology • U.S. Department of Commerce

Published in final edited form as:
J Vac Sci Technol A. 2019 ; 37: .

Measured relationship between thermodynamic pressure and refractivity for six candidate gases in laser barometry

Patrick F. Egan[1,a)], **Jack A. Stone**[1], **Julia K. Scherschligt**[1], **Allan H. Harvey**[2]

[1]Sensor Science Division, National Institute of Standards and Technology, 100 Bureau Dr, Gaithersburg, Maryland 20899

[2]Applied Chemicals and Materials Division, National Institute of Standards and Technology, 325 Broadway, Boulder, Colorado 80305

Abstract

Laser refractometers are approaching accuracy levels where gas pressures in the range 1 Pa < p < 1 MPa inferred by measurements of gas refractivity at a known temperature will be competitive with the best existing pressure standards and sensors. Here, the authors develop the relationship between pressure and refractivity $p = c_1 \cdot (n-1) + c_2 \cdot (n-1)^2 + c_3 \cdot (n-1)^3 + \cdots$, via measurement at T = 293.1529(13) K and λ = 632.9908(2) nm for $p \leq$ 500 kPa. The authors give values of the coefficients c_1, c_2, c_3 for six gases: Ne, Ar, Xe, N_2, CO_2, and N_2O. For each gas, the resulting molar polarizability $A_R \equiv \frac{2RT}{3c_1}$ has a standard uncertainty within $16 \times 10^{-6} \cdot A_R$. In these experiments, pressure was realized via measurements of helium refractivity at a known temperature: for He, the relationship between pressure and refractivity is known through calculation much more accurately than it can presently be measured. This feature allowed them to calibrate a pressure transducer *in situ* with helium and subsequently use the transducer to accurately gage the relationship between pressure and refractivity on an isotherm for other gases of interest.

I. INTRODUCTION

A. Background

Twenty years ago, Moldover[1] proposed a pressure standard based on the equation of state and ideal gas law $p = \rho RT$, where R is the molar gas constant and T is the thermodynamic temperature. At that time, the most promising method of determining gas density ρ was to infer it through measurements of the dielectric constant (i.e., capacitance) combined with the Clausius–Mossotti relation in electrostatics, which, for a nonpolar gas, relates the dielectric constant to density via the molar polarizability. A primary standard of pressure would use helium, because the polarizability of helium (and its deviations from ideal gas behavior) is calculable from first principles; calculations which, at the time, were approaching an accuracy comparable with the best experimental determinations.

a) patrick.egan@nist.gov.

This idea of using measurements of gas density to determine thermodynamic quantities was later taken up by Pendrill,[2] who gave particular attention to laser interferometry and measurements of gas refractivity as an alternative to measurements of permittivity by a capacitance bridge. (In electrodynamics, the Lorentz–Lorenz equation is the equivalent of the Clausius–Mossotti relation.) In 2004, at the time of Pendrill's review, the most accurate laser refractometers were measuring air refractivity with about 10^{-4} relative uncertainty; in terms of helium density inferred by measurement of refractivity, these levels of accuracy corresponded to a factor of 500 worse than state-of-the-art pressure standards (e.g., ultrasonic mercury manometers[3,4]). However, shortly after Pendrill's review, Stone and Stejskal[5] described a method to correct the errors in a laser refractometer using helium as a standard of refractivity. Although this approach of using helium for correction precludes primary realization of the pascal, it is of great practical use, a point to which we will return.

In 2007, Schmidt *et al.*[6] demonstrated the first sub-$10^{-5} \cdot p$ realization of the pascal in the equation of state, where density was inferred by microwave measurements of helium refractivity for $p > 1$ MPa. Pressure-induced distortion in the microwave resonator was corrected as isothermal compressibility, where the bulk modulus of the steel from which the resonator was made was measured within 0.08% by resonant ultrasound spectroscopy. Spurred by the achievement of Schmidt *et al.*, and the recent drive to determine Boltzmann's constant through helium density,[7] the twenty years since Moldover's original proposal[1] have seen theorists push uncertainties in the first-principles calculations of helium such that today, the relationship between thermodynamic pressure and refractivity is known within 10^{-6} for pressures up to 3 MPa.[8] Although theory and calculation of helium properties have set the stage for realization of the thermodynamic pascal within 1 μPa/Pa, at optical frequencies experiment presently lags theory by more than an order of magnitude.

We recently reported on a laser refractometer called MIRE (Ref. 9) that could realize the pascal to within 11.7 μPa/Pa standard uncertainty by measurement of helium refractivity at a known temperature. The refractometer principle was measurement of the change in optical path length through a gas cell in a heterodyne interferometer when the cell was filled with helium gas. Pressure-induced distortions in the cell windows were canceled by performing measurements of cells of identical geometry except for differing lengths, but uncertainty in the cancellation remained more than two times larger than the next largest uncertainty component. Nevertheless, as a working standard of pressure we would advise against this primary method of pascal realization, and instead advocate for a refractometer design based on a Fabry–Perot (FP) cavity.[5,10,11] Such a device typically has a systematic distortion error of 0.3% (for measurement of helium refractivity), but the error is reproducible at the 1 μPa/Pa level (for measurement of nitrogen refractivity), and the FP refractometer has several other points in its favor. One of the major attractions of using an FP refractometer is its sensitivity in the low-pressure range. In the past FP refractometry work,[12] we have demonstrated sub-mPa sensitivities, noise levels of 2×10^{-9} at atmospheric pressure, and linearity of the order of 1 part in 10^6, which allowed a transfer of the pascal to $p < 1$ kPa more accurate than the current primary realization (i.e., mercury manometer). Microwave and capacitance measurements do not perform as well in the low-pressure range at room temperature; neither does a non-resonant interferometer like MIRE. (The underlying difference between MIRE and an FP refractometer is that the latter can split a fringe with

exquisite precision.[13]) Additionally, the FP refractometer is a fairly simple device, and amenable to commercialization/deployment, whereas MIRE is a delicate instrument and complicated to build. Lastly, gas metrology instruments can often be limited by thermal-settling times due to pV-work[14] of the order of several hours for pressures up to 1 MPa; the FP refractometer can be designed for the optimal speed of response by minimizing gas volume and tightly enclosing the beam path between the mirrors in copper. However, in order for an FP refractometer to avail of its advantages over existing technologies in the low-pressure range, it is necessary to correct for the systematic distortion error.

There are a number of ways to correct the distortion,[15] and perhaps the most practical is the "two-gas method." For the two-gas method, a one-time calibration of the measuring instrument (the refractometer) would be implemented by performing two measurements of two gases of known refractivity as a function of pressure, with error in the refractometer being deduced as the unknown term common to both measurements. There would be no need for an accurate measure of pressure in this calibration procedure; it is only important that the pressure be the same for the two gas refractivity measurements. In this case, a refractometer such as that proposed by Stone and Stejskal would be disseminating the pascal via the optical properties of gases. Measurement traceability would be coming from whatever barometer was used to measure pressure when the relationship between pressure and refractivity was determined for the second gas. (The first gas could be helium, whose refractivity as a function of pressure comes from calculation. It is advantageous in the procedure that the ratio between two known refractivities is large: irreproducibility in the "same" pressure generated for the two gas measurements affects the correction inversely proportional to the ratio between the two refractivities.) It is our conceit that if the relationship between pressure and refractivity is determined for the second gas on the thermodynamic pressure scale, a refractometer whose errors are corrected by measurements of two gases can perform as a semiprimary[16] standard of pressure.

It is the purpose of this work to measure the relationship between pressure and refractivity for several gases that we consider good candidates for laser barometry. In these experiments, we use an off-the-shelf transducer to measure pressure. This transducer is calibrated by measurements of helium refractivity at a known temperature; theory is used to realize pressure in the equation of state (refractivity is the proxy for density). The calibrated transducer is subsequently used to record pressure when we measure the relationship between pressure and refractivity for other gases of interest. The physical property we are interrogating is molar polarizability, and our $16 \times 10^{-6} \cdot A_R$ performance is currently limited by how accurately we can calibrate a pressure gage by measurements of helium refractivity and realize pressure.

One last introductory note: In this work, we refer to "thermodynamic" and "mechanical" pressure. This is to distinguish two separate traceability chains for the derived unit of pressure:[17] the "thermodynamic pascal" has units Pa = J/m^3 and is traceable to Boltzmann's constant and the kelvin; the "mechanical pascal" has units Pa = N/m^2 and is traceable to Planck's constant and the kilogram.

B. Pressure and optical refractivity

In a real gas, the deviations from ideal gas behavior can be very closely approximated by a virial expansion in the molar density ρ

$$p = \rho RT(1 + B_\rho \rho + C_\rho \rho^2 + \cdots), \quad (1)$$

where p is the pressure, T is the thermodynamic temperature, and molar gas constant $R = k_B \cdot N_A$ is the product of Boltzmann's constant k_B and the Avogadro number N_A. In the revised SI, R has no uncertainty.[18] The density virial coefficients B_ρ and C_ρ can be calculated for helium[19–21] more accurately than any of the other terms in (1) can be measured. Moldover[1] anticipated this development in highly accurate calculation, which led him to propose a primary pressure standard based on (inferred) measurements of helium density. For gases other than helium, at present, the density virial coefficients at ambient temperature can be measured more accurately than they can be calculated.

There are a number of ways to get the density in (1), either by direct measurement (e.g., densimeter[22]) or inferred measurement (e.g., permittivity[1] or refractivity[6]). In the case of laser barometry which concerns this work, we infer density through measurements of refractivity $n - 1$ and the Lorentz–Lorenz equation

$$\frac{n^2 - 1}{n^2 + 2} = \rho(A_R + B_R \rho + C_R \rho^2 + \cdots), \quad (2)$$

where the molar polarizability term $A_R = \frac{4\pi}{3} N_A(\alpha + \chi)$ is dominant and depends upon the polarizability α and magnetic susceptibility χ of an atom/molecule. The deviations from linearity caused by interactions between atoms/molecules are taken into account by refractivity virial coefficients B_R and C_R. Again for helium, the molar polarizability and refractivity virial coefficients can be calculated[8] more accurately than they can be measured; whereas for other gases, measurements are more accurate than the present theory.

By the use of inverse series and series reversions, the common term density ρ can be eliminated from (1) and (2) so that pressure can be expressed as a power series of refractivity

$$p = c_1 \cdot (n - 1) + c_2 \cdot (n - 1)^2 + c_3 \cdot (n - 1)^3, \quad (3)$$

with

$$
\begin{aligned}
c_1 &= \frac{2RT}{3A_R}, \\
c_2 &= \frac{RT}{9A_R^3}(-A_R^2 + 4A_R B_\rho - 4B_R), \\
c_3 &= \frac{4RT}{27A_R^5}(-A_R^4 - A_R^3 B_\rho + A_R^2 B_R - 4A_R B_R B_\rho \\
&\quad + 4B_R^2 + 2A_R^2 C_\rho - 2A_R C_R).
\end{aligned} \tag{4}
$$

Here, we have used a series expansion in $n - 1$ for the Lorentz–Lorenz factor $(n^2 - 1)/(n^2 + 2) \equiv r(r + 2)/[r(r + 2) + 3] = 2r/3 - r^2/9 - 4r^3/27 + \cdots$ with $r = n - 1$ and kept terms up to third-order. For the highest refractivity measured in this work, Xe at 500 kPa and 293 K has $n - 1 \approx 3.3 \times 10^{-3}$, and the third-order expansion in $n - 1$ differs from the Lorentz–Lorenz factor by less than 8×10^{-9} fractional; the third-order approximation is accurate to within 10^{-6} for $n - 1 < 1.5 \times 10^{-2}$. Although it is more exact (and customary, as is done in refractive-index gas thermometry[23]) to expand (1) in terms of the Lorentz–Lorenz factor, for our interest in a pressure standard based on measurements of refractivity, an approximate expansion in $n - 1$ and the form of (3) has practical advantages.

By measuring refractivity as a function of pressure and fitting the experimental data with (3), we extract molar polarizability A_R, given by c_1. In principle, this parameter extraction can also arrive at a determination of either density or refractivity virial coefficients in (4), if the other is known. We do not attempt that in this work, and instead treat c_2 and c_3 as lump-parameters; we provide the $n - 1$, p, and T data as the supplementary material[24] which could be analyzed in other ways. (The values we obtained for c_1, c_2, and c_3 are given in Table I; procedure and analysis is discussed below.) Recent high-accuracy measurements of the refractivity virial coefficients at laser frequency are scarce, and most knowledge about them comes from work a generation ago.[25–27] Reference-quality equations of state (i.e., density virial coefficients) are an area of active research, such as in the densimeter of McLinden and Lösch-Will,[28] though their present levels of accuracy are only marginally good enough to say anything meaningful about the refractivity virial coefficient B_R. The motivation behind this work is to provide lump-parameter proportionality coefficients that relate gas refractivity to thermodynamic pressure, valid for pressures up to 500 kPa.

C. Comment on our choice of candidate gases

There are several practical problems in using helium in gas metrology (e.g., as a primary measurement standard of pressure): (1) its low polarizability and $\frac{\mathrm{d}n}{\mathrm{d}p} \approx 3.2 \times 10^{-10}$/pa at room temperature mean that pressure-induced distortions represent a relatively large systematic error; (2) low $\frac{\mathrm{d}n \cdot L}{\mathrm{d}p}$ sensitivity, compared to typical thermal and material instabilities in a refractometer cell/cavity of length $L \approx 0.25$ m, limits its low-end pressure range; (3) its relatively low polarizability also means that it is highly sensitive to contaminants, and special gas-handling procedures are required to ensure purity; (4) it has

small abundance, and higher cost; (5) helium permeates into some materials[29] and changes dimensions, which can be a deleterious effect in a refractometer that is, at heart, an ultrastable length metric. Thus, attractive alternatives to He would have high polarizability and low sensitivity to typical contaminants. It is also important that the gas be widely available in ultrahigh purity so that the pascal can be disseminated with assurance (that is, a measured relationship between refractivity and pressure for a specific gas, as reported here, can only be reproduced by an end-user with access to the same grade of purity). Another practical requirement is that a candidate gas should be neither toxic nor flammable.

These requirements directed our choice toward argon and nitrogen, both of which are widely available in 99.9999% purity and have $\frac{\mathrm{d}n}{\mathrm{d}p}$ about 8 times larger than He. Nitrous oxide has $\frac{\mathrm{d}n}{\mathrm{d}p}$ about 14 times larger than He, and it is possible (though difficult) to obtain in 99.9999% purity; however, the polarizability of N_2O is much higher than typical contaminants (water vapor, air, etc.) and its use in laser barometry would be more sensitive to things like outgassing. We also note that N_2O is not inert (a strong oxidizer), which is another possible disadvantage. Xenon is an inert gas with high polarizability, but it is expensive and we could not find purity higher than 99.9995%. We also chose to study two other gases, for different reasons. Calculations of the polarizability of neon within $8 \times 10^{-3} \cdot A_R$ are more than a decade old[30] and might be improved upon by recent developments in theory and computation; the present measurements could serve as a useful benchmark value on the frequency dependence of polarizability; the static polarizability of Ne has recently been measured[31] with much lower uncertainty than what is reported here. Lastly, carbon dioxide is another gas with relatively high polarizability but not available to us in purity greater than 99.9995%; however, CO_2 is of interest because its absorption line intensity, from which one can deduce ρ, can be calculated and measured with lower than 5×10^{-3} relative uncertainty: [32] one can imagine an interesting experiment that would compare, simultaneously in the same optical resonator filled with CO_2 to a few pascal, a pressure realized by refractometry with a red laser system to a pressure realized by spectroscopy with an infrared laser system.

II. GAS METROLOGY: APPARATUS FOR $n - 1$, p, T MEASUREMENT

We used the MIRE apparatus to measure gas refractivity. Our procedure was first to use MIRE to make measurements of helium refractivity at a known temperature, and solve for pressure in (3) using theory to evaluate the parameters of (4). This realization of thermodynamic pressure was compared to the reading of a pressure transducer, and a calibration look-up table was produced for the transducer at multiple pressures up to 500 kPa. This calibrated pressure transducer was then used to record the pressure of the six candidate gases when their refractivity was measured with MIRE.

In this section, we first describe the MIRE apparatus and associated instrumentation for measuring the relationship between pressure and refractivity on an isotherm. We end the section with a summary of the combined uncertainty in determining A_R.

A. Refractometer

A schematic of our gas metrology system is shown in Fig. 1. The central component of the system is the MIRE apparatus, which was reported in more detail in Ref. 9. (The optical scheme in Fig. 1 is for illustrative purposes only; Ref. 9 shows the actual layout.)

In addition to the basic gas plumbing shown in Fig. 1, some other details are relevant. The entire MIRE apparatus sat inside a stainless steel vacuum chamber with its own pumping system (not shown in Fig. 1). This 20 L chamber was continuously pumped with a roots-backed turbopump. There is no real requirement on vacuum in the chamber: vacuum is merely a convenient method of isolating the MIRE apparatus from fluctuations in temperature, and the thermal gradients that may develop across the optics through which the interferometer arms pass. However, for completeness, the vacuum level was typically (18 ± 5) mPa when monitored with a thermal conductivity gage. The vacuum reference cells in the MIRE apparatus (i.e., the two outer cells) do have moderate requirement on the stability of vacuum: fluctuations of residual gas in these cells would cause an error when refractivity measurements are carried out by filling the inner cell with gas. The vacuum reference cells have their own diaphragm-backed turbopump, and are continuously pumped through a 5 mm inner diameter tube, about 3 m in length. We monitored the vacuum with a thermal conductivity gage, and the level of vacuum was below the 1 mPa scale limit of the gage. The accuracy on this reading is not critical, and the ±10% specification by the manufacturer was good enough to confirm that the level of residual gas and fluctuations in the vacuum reference paths was insignificant to the accuracy of refractivity measurements made when the inner cell was filled with gas. (The largest conceivable error would be present when measuring 50 kPa helium: 1 mPa of water vapor in the outer cells represents an error of 1 part in 10^7.) The gas filling and plumbing arrangement for the inner cell is shown in Fig. 1 and also had its own diaphragm-backed turbopump. The angle-valve nearest the turbopump had greater than 5 mm inner diameter so that overnight pumpdown of the inner cell did indeed achieve a reliable “zero.” Again, quality of vacuum was evaluated with a thermal conductivity gage, which (after 12 h pumpdown) read below the 1 mPa scale limit of the gage. Gas purity was ensured by the conventional means of purging, dilution, and flow. The gas inlet and outlet on the triple-cell allowed flow throughout the entire plumbing volume, out of the gas cylinder into the turbopump. (The gas volume was about 0.2 L, evenly split between the inner cell of MIRE and the inlet/outlet gas lines.) The $n - 1$, p, and T measurements were performed at static pressure; the plumbing had no automatic flow control. The inlet/outlet flanges were clamped onto the glass with silicone o-rings: as noted above, the high vacuum in the chamber meant that these o-rings had no surrounding media that could permeate into the inner cell (all other fittings on the inlet/outlet lines in air were copper-gasket seals). “Outgassing” in the inner cell was evaluated by closing the valve to the turbopump after an overnight pumpdown, and monitoring the increase in pressure with a thermal conductivity gage. The increase in pressure was about 40 mPa/h: if the outgassing were of a species different from the measurement gas, this outgassing load is a potential error. However, even in helium (the measurement gas most prone to error arising from contamination), the accuracy of the refractivity measurement appeared independent of time [after thermal settling, see Fig. 2(c), discussed below]. One possible explanation of this feature is that the bore of the inner cell is a ground glass finish, and suboptimum for fast

pumpdown times (i.e., the observed outgassing was the slow release of the measurement gas from the rough glass surface).

MIRE consists of a gas triple-cell integrated into a differential heterodyne interferometer. The optical arrangement is such that twice the optical length of an inner cell is compared to the combined lengths of two adjacent outer cells. Either the inner cell or the two outer cells can be filled with gas while the other is maintained at vacuum. Refractivity in the gas-filled cell is deduced from

$$n - 1 = \frac{(2\pi N + \Delta\phi) \cdot \lambda}{8\pi L} - \frac{2d_{\mathrm{w}} \cdot p}{L}, \quad (5)$$

where $\Delta\phi$ is the phase change in the interferometer and is what is actually measured (with a phase meter) when the cell is filled with gas. To measure refractivity, MIRE has all three cells pumped to vacuum and the phase difference in the interferometer paths is measured; then the center cell is filled with gas to some pressure, and the phase difference between the interferometer paths is measured once more; this change in phase is $\Delta\phi$, which is some fraction of an interference fringe. If the relationship between refractivity and pressure (chiefly, polarizability) is uncertain at the 0.1%-level, the integer change in fringe N must be counted for several pressures along an isotherm; however, once the relation is established, it is much more practical for repetitious and wide-ranging datasets to note the change in pressure and instantly determine N numerically. (For these measurements, literature data on gas properties were quasiaccurate enough to determine N numerically: small adjustments were needed to the second-order term for Xe, CO_2, and N_2O to correctly identify N at higher pressures.) The vacuum-wavelength λ in the interferometer was calibrated by comparison to an iodine-stabilized laser, but even without this calibration its contribution to measurement uncertainty would only be a few 10^{-6} $(n - 1)$; see Ref. 33. The length of the triple-cell $L \approx$ 254 mm was measured with a coordinate-measuring machine. The change in path length d_{w} caused by increasing pressure on the cell window is by far the largest contributor to $u(n - 1)$. [Throughout this article, we use the notation $u(x)$ to denote the standard uncertainty of the quantity x. Unless otherwise stated, all uncertainties in this work are one standard uncertainty, corresponding to a 68% confidence level.] For our case of one pass through one window, d_{w} = 23.75(37) fm/Pa; the error is discussed in more detail in Appendix A. We estimated d_{w} by making relative refractivity measurements in triple-cells whose lengths differ by about 23 cm, but which both have nominally the same end-effect. (Similar end-effects mean almost identical end geometries, material properties, and position of the beams through all pairs of windows.) The concept behind the correction was to make the error common to measurements in triple-cells of different lengths so that it could be deduced through relative measurements of refractivity between long and short triple-cells. Relative measurements between long and short triple-cells need only be done once to determine the correction, and these were performed in Ref. 9; the refractivity measurements reported in this article solely employed the long triple-cell. When measuring gas refractivity, standard uncertainty in MIRE can be written as $u(n - 1) = [(5.5 \times 10^{-10})^2 + (3.1 \times 10^{-15} \cdot p)^2]^{1/2}$, where the pressure p unit is in pascal. The offset term is chiefly due to path length instability in the interferometer. The second term is pressure-dependent and chiefly due to uncertainty

in the window path length distortion $u(d_w)$; the overall contribution of this end-effect is inversely proportional to cell length, and the change in refractive index as a function of pressure $\frac{dn}{dp}$.

Lastly, we note that an alternate cell design[34] can potentially reduce the effect of d_w by a factor of 6, as well as allow measurement of pressures beyond 3 MPa over a range of (20 ± 50) °C; this new cell-based refractometer is currently in the planning stages. The 500 kPa pressure limit in the current MIRE is imposed by the risk of fracture to windows, which are only 3.4 mm thick and on a 19.1 mm diameter bore.

B. Barometer

We used measurements of helium refractivity by (5) in MIRE at a known temperature to realize thermodynamic pressure in (3). The uncertainty in this realization depends mainly on $u(n-1)_{He}$ as discussed above, but there are additional contributions from gas impurities and temperature measurement. A more in-depth analysis of uncertainty in the pressure realization is given in Ref. 9, which we can state here as $u(p_{MIRE}) = [(0.6\ \text{Pa})^2 + (11.7 \times 10^{-6} \cdot p)^2]^{1/2}$. As mentioned above, the offset term arises from instabilities in interferometer phase, which for helium becomes dominant at $p < 60$ kPa; the term proportional to pressure is chiefly due to $u(d_w)$, which for helium has a 9.8 μPa/Pa contribution. This realization of thermodynamic pressure was used to calibrate three off-the-shelf pressure transducers, which are all based on the same principle (i.e., strain applied to a quartz oscillator by a Bourdon tube and/or bellows). The three transducers operate in absolute mode only and have different upper ranges 110 kPa, 310 kPa, and 1380 kPa. The transducers measured pressure simultaneously, though we had to valve-off the lower-range transducer(s) when measuring higher pressures. The response of the transducers to pressure was independent of gas species; the only surfaces wetted inside the transducer were stainless steel. We calibrated these transducers on the thermodynamic pressure scale within the uncertainty $u(p_{MIRE})$; in use, however, the performance of the transducers added additional uncertainty when subsequently used to gage pressure as a function of refractivity for other gases of interest. Our final uncertainty claim in pressure (i.e., calibrated transducers in actual use) is about 10 times lower than what is specified by the instrument manufacturer, and it is thus worth a few remarks on some aspects of transducer performance.

The calibration data for each transducer are shown in Fig. 2(a), where the y-axis is the absolute value of the difference between the transducer reading and pressure realized by measurement of helium refractivity at a known temperature in MIRE. Each gage is identified by its maximum range in kilopascal, denoted p_{110}, p_{310}, and p_{1380}. We note that relative to p_{MIRE}, the p_{110}-gage reading was low, whereas the readings for the p_{310}- and p_{1380}-gages were high: although all three gages feature a transducer working on the same principle, the p_{110}-gage is from a manufacturer different than the other two gages. The error bars span $\pm\sigma$, where σ is the standard deviation on 10 repeat calibrations of each gage. The uncertainty in thermodynamic pressure $u(p_{MIRE})$ is plotted as the dashed line. The corrections measured in helium were applied to the gages on a point-by-point basis when measuring pressures of other gases. For the p_{1380}-gage, the calibration data are in reasonable agreement with a quadratic fit typical for such a transducer. In Fig. 2(a), we also show a second quadratic fit to

(not shown) calibration data; these separate gage calibrations are spaced 152 days apart. These differences in calibration factors are within 2 μPa/Pa; the ability to recalibrate the gages *in situ*, and update the calibration look-up table was one of the strengths of our procedure. However, the p_{310}-gage showed unexpected behavior, with notably larger error bars and poorer performance, which will be described next. Because of this poor performance, we did not use the p_{310}-gage reading for pressure measurement.

The poor performance of the p_{310}-gage appeared related to hysteresis and relaxation. At pressures below 110 kPa a relaxation of 15 μPa/Pa over 2 h was evident: the relaxation could be seen when simultaneously cycling all three gages between high vacuum and pressure and monitoring disagreement between the gages. (Previous studies we performed with the p_{110}-gage and a piston gage showed less than 2 μPa/Pa settling and hysteresis.) Relaxation could probably be dealt with by careful experimental procedure and timed data-taking. However, for pressures above 110 kPa hysteresis in the p_{310}-gage became a dominant and unpredictable error on the order of 2 Pa. Hysteresis manifested itself most clearly as irreproducibility in the vacuum-zero reading of the gage. In Fig. 2(b), we plot the vacuum-zero reading of each gage during a three-week measurement run. In the first four days, helium calibrations were performed up to 110 kPa for all three gages: the daily reproducibility in the zero of each gage was below 0.5 Pa, with the p_{110}-gage performing best. After the fourth day, the p_{110}-gage was valved-off and pressures between 140 kPa and 290 kPa were calibrated for the other two gages. The daily zero of the p_{310}-gage became irreproducible, with daily fluctuations up to 2 Pa, and therefore in this intermediate range we have more confidence in the p_{1380}-gage as a reliable measure of pressure. After the eleventh day, both the p_{110}- and p_{310}-gages were valved-off and the p_{1380}-gage was calibrated for pressures between 320 kPa and 500 kPa. Also note that for comparison in Fig. 2(b), the daily reading in MIRE phase at vacuum is also plotted as p_{MIRE}, where interferometric phase has been converted to helium pressure by $\frac{\mathrm{d}\phi}{\mathrm{d}p} = 3.2\,\mathrm{mrad/Pa}$. For p_{MIRE}, these daily zero fluctuations correspond to the remarkable stability of ±50 pm per day on a total path length of approximately 1.5 m.

The p_{MIRE} data in Fig. 2(b) should be taken as best-case. Stability of the phase difference in the interferometer depends most obviously on stable path lengths and/or common-mode immunity to fluctuation. MIRE has one small glass imbalance in its path length which can induce 26 pm/mK changes. The path length phase difference also depends on portion of the wavefront detected, and phase shift through transimpedance amplifiers and electronics. Additionally, stick-slip distortion of the interferometer baseplate is likely, since it is on a three-ball mount which rests on an aluminum plate in a stainless steel chamber; stick-slip changes in cell length are a negligible effect. Thus, interferometer stability is overall temperature dependent, though the relationship is not straightforward to model. As an example, during one outage in environment control, lab temperature increased by 3 K for 2 h, and over the next 12 h interferometer temperature increased 10 mK and the vacuum zero p_{MIRE} shifted 6 Pa, and did not return to its preinterruption reading. Nevertheless, for optimal experimental conditions, the p_{MIRE} data in Fig. 2(b) are representative. The pressure gages are also temperature-sensitive and we observed anomalous behavior in the zero reading of up to 0.5 Pa/K when lab temperature went out of control, worst-case being for the

p_{110}-gage. During typical operation, our lab temperature was stabilized to (19.5 ± 0.05) °C and MIRE was heated to 20 °C.

When measuring pressure of a gas, we recorded the gage reading in the experiment, and to this added the gage error calibration factor, the daily zero, and the head correction in postprocessing. Based on the above diagnostics we are confident that, after calibration by measurement of helium refractivity at a known temperature, the performance of the p_{110} and p_{1380} gages do not add more than $[(0.5\ \text{Pa})^2 + (8 \times 10^{-6} \cdot p)^2]^{1/2}$ standard uncertainty to the measurement of pressure. The offset term was evaluated from the reproducibility in the gage reading at zero pressure; the term proportional to pressure does account for small fluctuations in the scale of the gage between *in situ* calibrations, but was chiefly based on the observation that residuals and standard deviation in the fit to (3) appeared independent of polarizability. [This feature is evident in Fig. 3(b): the relative error in $n - 1$ measured by MIRE decreases proportional to the magnitude of $\frac{\mathrm{d}n}{\mathrm{d}p}$, and therefore the similar standard deviations across all gas species indicate random error in either thermometry or barometry; we do not believe these random errors arise from the temperature measurement system, as described next.] Our combined standard uncertainty for measuring the pressure of candidate gases is thus $u(p)$ $[(0.8\ \text{Pa})^2 + (14.2 \times 10^{-6} \cdot p)^2]^{1/2}$, and is about 4 times lower than pioneering work in gas metrology[35,36] using a transducer working on the same principle. Our claim on performance of these pressure gages is at the limit of what is feasible: It must be emphasized that (1) the gages were calibrated in place with helium gas and remained untouched when refractivity measurements of other gases were performed, (2) daily vacuum zeros were recorded, and (3) that our lab was temperature-stabilized.

C. Thermometer

Gas temperature was measured by type-T thermocouples (differential configuration) and a calibrated thermistor with a resistance bridge. The thermometer was calibrated on the International Temperature Scale of 1990 (ITS-90). The thermistor was located in a thermowell inside an aluminum block into which the thermocouple reference junctions were epoxied; the thermowell was on the “air-side,” and thus the thermistor experienced neither changes in pressure nor gas species; Fig. 1 illustrates the thermometry configuration. The thermocouples sensed the difference in temperature between the reference junction and the triple-cell (in vacuum); the thermocouples were in vacuum and also experienced neither changes in pressure nor gas species. Offsets (0.25 mK) in this thermocouple arrangement were zeroed by placing the sense junctions inside the block which houses the reference junctions and thermistor (the offsets were most likely electrical since when its terminals were shorted, the nanovoltmeter still read nonzero). The accuracy of our isotherm is thus a combined uncertainty of thermometer calibration, nanovoltmeter drift, and difference between ITS-90 and thermodynamic temperature.[37] The thermocouple reading at the triple-cell was typically within ±2 mK of the thermistor (reference junction), but filling the cell caused a temperature increase with a settling time of about 2 h, before which refractivity and/or gas temperature could not reliably be measured. The process of gas filling and subsequent wait-time (settling) raises several possible concerns: (1) thermal gradients induced across the triple-cell windows, which would not cancel between reference and measurement optical path lengths, (2) permeation of helium into the windows that would

change the refractive index of the glass, which also would not cancel between reference and measurement optical path lengths, and (3) contamination of the helium due to outgassing. In Fig. 2(c), we show the pressure error and temperature transients over 10 h after a 440 kPa fill of helium. A finite-element model of the problem aids in understanding these transients, and relevant temperature probes are also plotted in Fig. 2(c); the finite-element model is discussed more in Appendix B. The large change in the fractional error of pressure at $t < 2$h is most likely dominated by thermal settling of the gradient between the thermocouple on glass and the beam path in (hot) gas; p_{MIRE} reads high at $t < 2$ h which is indicative of T_{cell} reading lower than actual gas temperature T_{gas}. Finite-element modeling also supports this interpretation, which showed a 2 mK gradient persisting between the gas and the point on the cell at which temperature was mea- sured $T_{\mathrm{gas}} - T_{\mathrm{cell}}$. On the other hand, the aforementioned temperature gradient across the window would cause the part of the window exposed to pV-work to heat up, and thereby decrease the refractive index in the measurement path; in this case, p_{MIRE} would read lower than what would be expected when the window is thermally uniform. Finite-element modeling showed gradients across the window $\Delta T_{\mathrm{window}}$ decreasing below 1 mK within 1 h; the thermooptic coefficient of borosilicate crown glass is about $\frac{\mathrm{d}n}{\mathrm{d}T} = 2.7 \times 10^{-9}/\mathrm{mK}$, and 1 mK gradients across the glass correspond to errors in inferred helium pressure of 0.12 Pa for 3.4 mm window thickness, which is a very small effect. After thermal settling $t > 2$ h, the standard deviation in the fractional error of pressure is less than 0.4 μPa/Pa: this stability is comparable to what would be expected from the temporal instability in the interferometer path length and/or the p_{1380}-gage reading [Fig. 2(b)] and gives us confidence that neither helium contamination nor permeation into glass are problems at this level of accuracy. In principle, all these effects—thermal settling, helium contamination, helium permeation—could be canceled by careful extrapolation as a function of time, but based on Fig. 2(c) we apply no extrapolation to our measurements of $n - 1$, p, or T. Indeed, Fig. 2(c) is a worst-case scenario for how long we had to wait before recording p_{MIRE}, which only applied for the first datapoint, after the triple-cell had been pumped to vacuum overnight: subsequent datapoints in our measurement protocol, which consisted of rapid repeated pumping, flushing, and filling, showed settling times of the order of 1 h, and a typical pressure “step” was only 30 kPa or 60 kPa and not the 440 kPa of Fig. 2(c). Nevertheless, faster response times and less thermal disturbance would be desirable, and the seven times smaller gas volume of a new quadruple-cell apparatus[34] is another of its benefits.

D. Combined uncertainty $u(A_R)$

Lastly, one way to summarize the performance of our gas metrology system is to tabulate an uncertainty budget for how accurately we can extract molar polarizability A_R in (4) from measurement for each of the six candidate gases. This uncertainty budget is given in Table II. Uncertainty in A_R is dominated by uncertainty in pressure measurement $u(p)$, which reflects the accuracy of the gages in use after calibration by measurement of helium refractivity at a known temperature. For the heavier gases, our 0.5 cm uncertainty in head height contributed an additional few μPa/Pa to $u(p)$. Uncertainty in thermodynamic temperature $u(T)$ was 3.1 times smaller than $u(p)$. Uncertainty in the measurement of refractivity $u(n - 1)$ scales inversely proportional to polarizability, being 2.7 times smaller

than $u(p)$ for Ne, 10.9 times smaller than $u(p)$ for Ar, etc. Impurities in the gas samples were another small contribution to measurement uncertainty, which is largest in the case of Xe where uncertainty in gas purity has a contribution 4.8 times smaller than $u(p)$; impurity concentrations are stated in the supplementary material[24] to this article. A final uncertainty component was statistical and comes from the standard deviation on the residuals when (3) was regressed to the measured data (data analysis is discussed below). In summary, for all six gases the combined uncertainty in extracting A_R is dominated by $u(p)$. Additionally, the components $u(T)$ and $u(n-1)$ are correlated with $u(p)$, in the sense that they are accounted for in the helium calibration procedure for the pressure gages. However, we leave our uncertainty in A_R as slightly overestimated; if our uncertainty in pressure measurement were significantly reduced, a more careful case-by-case uncertainty analysis would be required for each gas.

III. RESULTS AND DISCUSSION

In this section, we first present the $n-1$, p, and T datasets and describe the procedure for obtaining proportionality coefficients between pressure and refractivity. The datasets for the six gases are provided as the supplementary material[24] to this article. We then analyze the datasets in terms of the Lorentz–Lorenz factor and density, where density is computed from the measured pressure and temperature using reference equations of state. We end the section with a comparison among literature measurements of A_R for each gas and some discussion.

A. Gas measurements and extracted coefficients

Gas refractivity measurements proceeded by stepping pressure through the range 50 kPa to 500 kPa in 30 kPa increments on the isotherm T_{90} = (293.15 ± 0.005) K. All pressure adjustments were done by hand, typically obtaining six or seven refractivity measurements per day with the plumbing configuration of Fig. 1; the datasets for the six gases took about eight months to acquire. For each pressure adjustment, we pumped out the old gas, flushed new gas through the triple-cell, and refilled to the new pressure; at the end of the day the apparatus was pumped to high vacuum (below 1 mPa) overnight, and new zero pressure readings were recorded the next day. As noted in Fig. 2(c), gas filling increased triple-cell temperature by approximately 0.15 mK/kPa, with a 2-h settling-time. Our procedure was to initially fill the cell, wait at pressure for a thermal settling period, and discard the initial datapoint; then we quickly pumped out the cell, flushed and re-filled to the same pressure and began recording data. In this way, the net energy increase in the system for a fill was small, and thermal-settling times more manageable; nevertheless, the process was slow and labor-intensive, and we would plan to automate future experiments.

In Fig. 3(a), we plot measurements of refractivity as a function of pressure for all six candidate gases. We adjusted the measured values of p to constant T_{90} = 293.15 K using $(\partial p/\partial T)_\rho$ for a real gas, and compensated for the typical ±5 mK excursions during a dataset about that isotherm. [For these small excursions, the difference between real gas behavior $(\partial p/\partial T)_\rho$ and the ideal gas approximation $\frac{\mathrm{d}p}{\mathrm{d}T}$ is up to $4 \times 10^{-7} \cdot p$/mK for the heaviest gases.] Equation (3) was then fit to the isothermal dataset, minimizing the total least-squares

for each gas by weighted orthogonal distance regression. The regression procedure used the algorithm ODRPACK[38] from the SciPy library. The ODRPACK allows weighting of the fit to be dependent upon uncertainty in both variables, p and $n - 1$; the weighting of the fit was the reciprocal of the square of the estimated uncertainty in each variable. For the variable p, we used the root-sum-square of the p and T uncertainties in Table II. For the variable $n - 1$, we used the root-sum-square of the $n - 1$ and impurity uncertainties in Table II. The residuals from the fit for each gas are plotted in Fig. 3(b); our notation $p(n - 1)_T$ signifies pressure as a function of refractivity at constant temperature, embodied in (3).

The proportionality coefficients extracted from the regression are listed in Table I. The coefficients are given for thermodynamic temperature, and we have applied the correction $T - T_{90}$ (2.9 ± 0.4) mK,[37] because our data were measured on ITS-90. The numbers in brackets in Table I are statistical uncertainties on the weighted orthogonal distance regression only. For c_1 this statistical uncertainty component has been included in Table II as the entry "regression." These statistical uncertainties were estimated as the square-root of the diagonal elements of the covariance matrix. Boggs *et al.*[38] advise caution when evaluating confidence by the covariance matrix, but concede that it is often adequate; readers interested in a more careful statistical analysis for the proportionality coefficients are encouraged to reanalyze our experimental data, which are provided as the supplementary material[24] to this article. We finally note the units for the proportionality coefficients come directly from measurement. Our choice to express the coefficients this way—i.e., pressure as a function of refractivity at constant temperature $p(n - 1)_T$, instead of the more typical $n(p, T)$—is driven by the practical concern of laser barometry which motivates this work: any refractometer operating at a similar wavelength and thermodynamic temperature can use a measurement of gas refractivity with c_1, c_2, and c_3 as stated to realize the pressure in (3). (As a general rule, most high-precision refractometers actually measure $n - 1$, as the change in refractive index from the known $n = 1$ of vacuum, and so expressing coefficients in terms of $n - 1$ is favored from the experimental point of view.)

One last point worth mentioning is that our regression to find A_R in (3) employs a third-order series expansion in $n - 1$ to approximate the Lorentz–Lorenz factor. If we perform a regression on a function $p = (RT/A_R) \cdot (n^2 - 1)/(n^2 + 2) + \cdots$ (the more exact expression), we obtained consistency between the extracted molar polarizabilities within $8 \times 10^{-7} \cdot A_R$. We are thus confident that the approximation of the Lorentz–Lorenz factor adds very small uncertainty when extracting A_R.

B. Equation of state analysis

In Fig. 4, we depict a more intuitive analysis of the data in terms of (2), where we plot the Lorentz–Lorenz quotient divided by density as a function of density on the x-axis. To convert measurements of p and T to ρ, we used the reference equation of state (EOS) for each gas as implemented in REFPROP.[39–44] For some of these gases, the EOS uses values of R that are now obsolete; this would mean that using ρ directly from REFPROP would result in offsets up to $6 \times 10^{-6} \cdot A_R$ in the y-axis of Fig. 4. In order to avoid these offsets in ρ-REFPROP, we instead calculate density

$$\rho = \frac{p}{ZRT}, \quad (6)$$

using the compressibility factor Z taken directly from REFPROP. In this procedure, the pressure in (6) has been adjusted to constant temperature using REFPROP $(\partial p/\partial T)_\rho$. The reference temperature to which we adjusted was $T = 293.1529$ K, which is $T_{90} = 293.15$ K with the current estimate of the correction $T - T_{90} = (2.9 \pm 0.4)$ mK;[37] if the difference between thermodynamic temperature and ITS-90 becomes better known in the future, our analysis would need to be adjusted to reflect best knowledge.

The y-axis of Fig. 4 corresponds to the relative deviation of the Lorentz–Lorenz quotient from A_R, which it should approach in the zero-density limit $\rho \to 0$. Our estimated value $A_R = \frac{2RT}{3c_1}$ for each gas is listed in Table III. For the dashed lines shown, we used linear least-squares fitting of a quadratic function to the EOS-processed data; for neon only, the quadratic term was statistically insignificant. The zoom plot of Fig. 4(b) shows relative deviation of the Lorentz–Lorenz quotient at $\rho \to 0$ from A_R within $1 \times 10^{-6} \cdot A_R$ for five out of six gases; the relative deviation for neon is $2 \times 10^{-6} \cdot A_R$. In the EOS analysis, the extrapolation of the measurements to $\rho \to 0$ is still dependent on a polynomial model $f(\rho) = a_0 + a_1 \cdot \rho + a_2 \cdot \rho^2 + \cdots$ that accounts for nonlinear effects due to refractivity virial coefficients and the inaccuracy of density virial coefficients implicit in the EOS. The situation for determining $a_0 \equiv A_R$ thus becomes analogous to extracting $c_1 = \frac{2RT}{3A_R}$ by the fitting of (3) to the $p(n-1)_T$ dataset, but finding a_0 is arguably less reliable. First, the value of ρ derived from the measurement of gas pressure and temperature is dependent on the choice of EOS. Second, as mentioned by Schmidt and Moldover,[36] "uncertainty in the ordinate diverges in proportion to $\frac{1}{\rho}$ as $\rho \to 0$." Thus, small deviations between a_0 and A_R are to be expected at the highest levels of accuracy. As pointed out by May *et al.*,[54,55] for the purposes of comparing polarizabilities between gases, finding A_R by regressing $p(n-1)_T$ has the advantage that errors caused by inaccuracies in the respective EOS would not contribute to a ratio of measured polarizabilities; on the other hand, if the interest is determining second-order effects (e.g., refractivity virial coefficient), correlations between c_2 and c_3 may lead to unreliable results, and in that case the EOS analysis provides a useful cross-check. For our interest in basing a pressure standard on measurements of refractivity, a regression to $p(n-1)_T$ is arguably the most appropriate approach, and thus in this article we have given clear preference to $A_R = \frac{2RT}{3c_1}$ and its application to (3).

C. Comparison with the literature

For neon and argon, our measured A_R can be compared with values derived from the recent high-accuracy static measurements of Gaiser and Fellmuth,[31] who reported $A_\epsilon^{\mathrm{Ne}} = 0.9947114(24)\,\mathrm{cm}^3/\mathrm{mol}$ and $A_\epsilon^{\mathrm{Ar}} = 4.140686(10)\,\mathrm{cm}^3/\mathrm{mol}$. To correct these static polarizabilities to optical frequencies, we use Cauchy moments derived from the dipole

oscillator strength distributions of Kumar and Thakkar;[56] they estimate the first two moments to have an uncertainty of 1% and the next two (the last of which makes a negligible contribution at 633 nm) to have an uncertainty of 3%. Finally, we add a small term corresponding to the magnetic susceptibilities χ reported by Barter *et al.*[57] The resulting values are $A_{\epsilon\to R}^{\mathrm{Ne}} = 1.00028(6)\ \mathrm{cm}^3/\mathrm{mol}$ and $A_{\epsilon\to R}^{\mathrm{Ar}} = 4.1956(6)\ \mathrm{cm}^3/\mathrm{mol}$, where in both cases the uncertainty is dominated by that of the dispersion correction from zero frequency to our measurement frequency. These $A_{\epsilon\to R}$ agree with our result for neon within mutual uncertainties, and are in excellent agreement with our result for argon, but our uncertainties in measurement are smaller than the uncertainty in the dispersion-corrected static values by roughly a factor of 4 for neon and a factor of 10 for argon.

From Table III, for neon agreement among experiments is not good: the three measurements of Birch, Achtermann *et al.*, and ours do not overlap within 1σ standard uncertainty; indeed, our disagreement with Birch is a little more than 15σ. Birch[47] claimed "uncertainty at the 99%" confidence level and stated an uncertainty of "≤ 2.0 parts per 10^4" for molar polarizability; we interpret this as a $k = 2.58$ expanded uncertainty and arrive at the 8×10^{-5} $\mathrm{cm}^3/\mathrm{mol}$ standard uncertainty noted in Table III for his measurement of neon. We can only speculate at to why there are profound disagreements in experiment: (1) It has long been known[5,8,58] that, for helium, the measurements of Birch (and Achtermann *et al.*) have been discrepant with theory, and this discrepancy has recently been verified experimentally[9] to be about 32σ; (2) Questions arise about the purity of the gases used in Birch (and Achtermann *et al.*), which for neon was claimed to be 99.995% in both cases; (3) Questions arise about the model used to correct path length errors due to window distortion: the model used by Birch treats the change in refractive index of the glass (due to the applied pressure) as proportional to change in density and does not account for radial and nonuniform stress components, and our work[9] (based on Shelton[59]) and the more recent work of Bartl *et al.*[60] show it to be wrong by up to a factor of 8; the model used by Achtermann *et al.* is purely geometric, treats the cell as a spring, and does not account for the change in path length through the glass windows. It is notable that for #2 above, most impurities in neon would lead to a measurement of neon refractivity appearing larger than it actually is. However, for #3 above, the sign of d_{w} depends on cell and pressure configuration: in our case of pressurizing a cell interior, which is the same configuration as was used by Birch and Achtermann *et al.*, d_{w} is a net decrease in optical path length through the window for increasing gas pressure, and hence not fully accounting for the effect would make a measurement of refractivity appear smaller than it actually is. (On the other hand, for the case of Bartl *et al.*[60] where the exterior of a cell is pressurized, there is a net increase in optical path length through the window.) Measurements of high $\frac{\mathrm{d}n}{\mathrm{d}p}$ gases are also instructive, because the effect of #3 above becomes proportionally smaller, whereas for #2 most impurities in xenon and nitrous oxide would lead to a measurement of refractivity appearing smaller than it actually is. For xenon, Achtermann *et al.* reported a purity of 99.99% and a measured polarizability 20σ lower than ours. These considerations suggest the possibility that disagreements may have arisen from impurities in the gas samples that were greater than believed, which would offer one explanation for discrepancies in the historical measurements of gas polarizabilities, evident in Table III. However, this line of reasoning

falters in the case of carbon dioxide and nitrous oxide; indeed, for N_2O, Birch used 99.997% purity and reported polarizability a little more than 3σ higher than our measurement, which is the opposite to what might be expected from the impurity reasoning above. (Impurity concentrations for each of our gas samples are given in the supplementary material[24]. Here, we state the grade specifications: Ne 99.9995%, Ar 99.9999%, Xe 99.9995%, N_2 99.9999%, CO_2 99.9995%, N_2O 99.9999%.)

Our measured proportionality coefficients for nitrogen and argon can be compared to previous measurements[50] made at the same wavelength and temperature, but in a different apparatus based on a Fabry–Perot (FP) refractometer. Our old measurements employed a pressure transducer calibrated against a mechanical pressure standard. The 2011 measurements, as listed in Table III, have been adjusted by $+19.3 \times 10^{-6} \cdot A_R$ to account for one bias and one bias-plus-blunder. The first bias is due to the difference between thermodynamic temperature and ITS-90; we reported Ref. 50 in ITS-90. The difference is presently estimated as $T - T_{90} = (2.9 \pm 0.4)$ mK at $T_{90} = 293.15$ K,[37] which corresponds to a $9.9 \times 10^{-6} \cdot A_R$ correction for both gases. The bias-plus-blunder concerns helium permeation into the FP refractometer, which changed its length when we attempted to correct for pressure-induced distortion. In practice, to disentangle pressure-induced distortion from the distortion due to helium permeation, one must extrapolate the length of the spacer back to the time immediately after a fill, where the pressure-induced distortion is apparent but the distortion due to helium permeation has not yet taken place. In 2011 it was not clear whether the observed nonlinear lengthening after a helium fill was due to permeation or some thermal transients. We therefore stated in Ref. 50 that we applied a correction halfway between a linear extrapolation and a quadratic fit; however, one of us (PFE) made a blunder and applied a linear extrapolation only. This bias-plus-blunder is compounded by the fact that more recent studies have shown that the geometric effect of helium permeation is indeed nonlinear,[11] and that the correct extrapolation would be modeled as diffusion $\beta \cdot \sqrt{t}$, where the diffusion parameter β depends on helium pressure and surface area of the FP cavity geometry. The effect of this mistake is that in reporting our measurements of nitrogen and argon refractivity, our calculation of A_R was too low by 9.4 parts in 10^6 for both gases. The net effect of these two biases ($T - T_{90}$ and blundered helium extrapolation) is a $+19.3 \times 10^{-6} \cdot A_R$ A_R correction for both gases. However, after applying this correction, agreement between the 2011 and present measurements is marginal. In hindsight, and with the experience of the barometer characterization work reported in this article, we now believe that our stated standard uncertainty of 0.8 Pa at atmospheric pressure in Ref. 50 for a mechanical barometer in use (after calibration, transport, temperature change, etc.) was optimistic. We also claim more confidence in the present measurements and reported polarizabilities in Table III, both because our pressure gage is calibrated at the point-of-use, and because our parameter extraction procedure does not rely on knowledge of density and refractivity virial coefficients to convert measurements of refractivity to molar polarizability. In Ref. 50 we used literature values to estimate density and refractivity virial coefficients and effectively extrapolated a measured refractivity near atmospheric pressure to the zero-density limit. The present data cover a much broader pressure range than 2011: density and refractivity virial coefficients are left as free parameters and the data are

regressed to the zero-density limit by (3). We consider the present measurements to supersede those of 2011.

For nitrogen we can also compare current measurements to recent, more accurate measurements,[12] which were also performed in an FP refractometer, albeit of different design than the one reported in Ref. 50. The 2016 measurements were performed at the same wavelength but different thermodynamic temperature $T = 302.919$ K. The 2016 measurements of $A_R^{N_2}$ are about 4 times more accurate than the present ones because nitrogen pressure was measured by a mercury manometer, one of the most accurate realizations of the mechanical pascal. The 2016 measurements yielded $c_1^{303\,K} = 3.7764715 \times 10^8$ Pa, $c_2^{303\,K} = -2.982 \times 10^8$ Pa and $c_3^{303\,K} = 1.24 \times 10^{10}$ Pa, valid for $p <$ 180 kPa. The two sets of proportionality coefficients measured at temperatures differing by 10 K can only be compared within the uncertainty of nitrogen refractivity and density virial coefficients, and the possible dependence of molar polarizability on temperature for the nitrogen molecule. Previous measurements for nitrogen over broader temperature ranges have estimated this dependence to be between $78(47) \times 10^{-7}$ (cm^3/mol)/K in Hohm and Kerl[46] at optical frequency, and $62(11) \times 10^{-7}$ (cm^3/mol)/K in Schmidt and Moldover[36] at the static limit. Harvey and Lemmon[61] reanalyzed the data from Ref. 36 and estimated a dependence of 82×10^{-7} (cm^3/mol)/K. The dependence has been calculated for optical frequency as $48(1) \times 10^{-7}$ (cm^3/mol)/K by Buldakov *et al.*[62] and for the static limit as 51×10^{-7} (cm^3/mol)/K by Sharipov *et al.*[63] We plot literature measurements of nitrogen polarizability in Fig. 5 across a 30 K range. A weighted least-squares fit on these measurements returns the slope 137×10^{-7} (cm^3/mol)/K, which is inconsistent with the previous (broader range) measurements and theory just mentioned; on the other hand, if only considering c_1 from the present measurement and $c_1^{303\,K}$ from the 2016 measurement, the dependence 33×10^{-7} (cm^3/mol)/K is closer to existing estimates. This discrepancy is one motivation behind our drive toward a new apparatus that will perform more accurate measurements of $A_R^{N_2}$ over a broader temperature range;[34] in the context of a pressure standard based on the molecular properties of nitrogen, a more accurate understanding of these properties appears necessary.

IV. CONCLUSION

We measured refractivity as a function of pressure for six gases, which are candidates for use in laser barometry. By fitting a third-order power series to the experimental data, we have determined the proportionality constants that relate pressure to refractivity. The first-order power term (the linear term) yielded values for molar polarizabilities within a standard uncertainty $16 \times 10^{-6} \cdot A_R$; for gases other than nitrogen, this is the first time molar polarizability at optical frequency has been measured to this level of accuracy. Consequently, a laser refractometer using one of these candidate gases near 293.153 K can now realize the pascal by a semiprimary method to within 16 μPa/Pa standard uncertainty, for pressures $p \leq$ 500 kPa. Errors in the refractometer can be canceled (calibrated) by measuring two or more

of these gases at the same (unknown) pressure and a known temperature. Traceability to the SI derived unit Pa = J/m^3 is provided via the optical properties of gases.

The field of laser barometry is a work in progress. A performance of 16 μPa/Pa is almost an order of magnitude worse than what can presently be realized with a mercury manometer for the mechanical pascal. We believe a next iteration of MIRE (Ref. 34) will reduce $u(p)$ by up to a factor of six, and operate across wider temperature and pressure ranges, but major work is needed to bring these speculative claims to fruition. Additionally, for practical pascal dissemination in the field, FP cavity refractometers will probably operate at telecom wavelength (e.g., around the acetylene absorption region near 1542 nm, which is a convenient vacuum-wavelength reference), and so more work is needed to accurately determine polarizability and refractivity virial coefficients at the lower optical frequencies. And lastly, for laser barometry and the thermodynamic pascal to gain a broader acceptance, it is necessary that measurements of $p(n-1)_T$ for these gases are repeated by other groups, ideally at levels of accuracy higher than what has been reported here.

Supplementary Material

Refer to Web version on PubMed Central for supplementary material.

ACKNOWLEDGMENTS

The authors thank K. Szalewicz at the University of Delaware for advice on correcting static polarizabilities to optical frequencies. They also thank A. Sharipov and B. Loukhovitski at the Central Institute of Aviation Motors, Moscow, for sharing the numbers underlying their graphical presentation of N_2 polarizability in Ref. 63. The authors understanding of window path length errors has benefited from discussions with G. Bartl and R. Schödel at the Physikalisch-Technische Bundesanstalt, Braunschweig; these interactions encouraged them to include Appendix A.

APPENDIX A:: CHANGE IN OPTICAL PATH LENGTH THROUGH A STRESSED WINDOW

The change in path length experienced by a laser beam passing one time through one window has been given by Shelton.[59] Our convention is shown in Fig. 6, and the expression for change in path length

$$d_w \cdot p = (n_i - 1) \cdot (w_f - w_i) + w_f \cdot (n_f - n_i), \quad \text{(A1)}$$

has terms describing the change in geometric thickness of the window from initial w_i to final w_f, and change in glass refractive index from initial n_i to final n_f, in response to a change in applied pressure p. Although $d_w \cdot p = w_f (n_f - 1) - w_i(n_i - 1)$ is the more compact expression, we keep consistent with the form of Shelton because it has the heuristic advantage of grouping together the changes in both effects, i.e., geometry and refractive index. In Fig. 6, the freespace length $L_2 - (w_f - w_i)$ should take into account the increase in path length caused by the increasing refractive index of the gas, implied by the increasing pressure; the corrections to (A1) would be (i) a term $(n_{gas} - 1)\, L_2$, which, in a refractometer, is the thing that is actually measured, and (ii) a term $(n_{gas} - 1)(w_f - w_i)$, which is on the order of 10

am/Pa—more than two orders of magnitude smaller than the path length change inside the window.

Shelton[59] used analytical expressions from elastic theory to estimate the change in geometry and stress experienced by a window under the applied pressure; the calculated stress was converted to change in refractive index based on photoelastic principles. Our procedure to calculate d_w is based on finite-element modeling (FEM): we use FEM to estimate (i) the change in geometric window thickness $w_f - w_i$, and (ii) the integrated stress along the beampath through the window; then, like Shelton, we employ the elasto-optic coefficients to convert stress to change in refractive index $n_f - n_i$. The use of FEM is less elegant than Shelton, but ought to be equally effective; indeed, from it we can obtain the geometry and integrated stress in a specific portion of the window (i.e., along the beampath), and easily account for nonsymmetric cases, such as MIRE.

The FEM change in geometric thickness through the window can be seen in Fig. 7(a). The profile of the window front and back surfaces where the beam passes through are extracted from the FEM and averaged. This process yields $(w_f - w_i)/p = -37.3$ fm=Pa for the inner beam passing through the inner cell (i.e., the cell exposed to an increase in pressure) and $(w_f - w_i)/p = -1.61$ fm=Pa for the outer beam (i.e., passing through the cell that remains at vacuum). Note the signs are in relation to the z-axis of the FEM in Fig. 7(a): the inner cell is becoming longer, the outer cell is becoming slightly shorter, and both the inner and outer beams pass through a window that is becoming geometrically thinner.

The change in refractive index experienced by the glass is calculated from

$$n_f - n_i = \frac{1}{2}\left[\frac{dn_\parallel}{d\sigma}(\sigma_x + \sigma_y) + \frac{dn_\perp}{d\sigma}(\sigma_x + \sigma_y + 2\sigma_z)\right], \quad \text{(A2)}$$

where $\sigma_{x,y,z}$ is the normal stress in the x, y, z axis; the FEM estimate of stress will be discussed momentarily. The change in refractive index in response to the applied stress is polarization-dependent and is given by

$$\begin{aligned} \frac{dn_\parallel}{d\sigma} &= -\frac{n^3}{2E}(p_{11} - 2\nu p_{12}), \\ \frac{dn_\perp}{d\sigma} &= -\frac{n^3}{2E}[-\nu p_{11} + (1-\nu)p_{12}], \end{aligned} \quad \text{(A3)}$$

where E is the elastic modulus and ν is Poisson's ratio. The elasto-optic (strain-optic) coefficients p_{11} and p_{12} are given in several textbooks (e.g., Ref. 64), which generally refer to the measurement technique of Borrelli and Miller.[65] For borosilicate crown, the glass from which the triple-cell is made, we use the measurements reported in Ref. 66 to discern $\frac{dn_\parallel}{d\sigma} = -3.0 \times 10^{-13}$/Pa and $\frac{dn_\perp}{d\sigma} = -2.76 \times 10^{-12}$/Pa. Note that these terms are signed: compression increases refractive index, and tension decreases refractive index. (We also

note, we chose borosilicate crown glass for ease of manufacture, and with the purpose of being over-cautious about helium absorption. A next-iteration design will be in fused silica, mostly to avail of its low coefficient of thermal expansion so that uncertainty in cell length does not contribute error when measuring $p(n-1)_T$ far from $T_{90} = 293.15$ K, the temperature at which the cell length can be accurately measured on a coordinate-measuring machine.)

The FEM result of normal stress along the beampath is shown in Figs. 7(b) and 7(c). The stress for each element in the regions shown is extracted from the FEM for each axis, and the average of the sum of all elements is used to obtain the integrated stress. The result for the inner beampath is $\sigma_x = 0.923$Pa/Pa, $\sigma_y = 1.006$Pa/Pa, and $\sigma_z = 0.507$Pa/Pa, and for the outer beampath $\sigma_x = 0.087$ Pa/Pa, $\sigma_y = 0.118$ Pa/Pa, and $\sigma_z = 0.002$ Pa/Pa. From these results and (A2), the change in refractive index through the beampath is $(n_f - n_i)/p = -1.64 \times 10^{-12}$/Pa for the inner beam, and $(n_f - n_i)/p = -3.19 \times 10^{-13}$/Pa for the outer beam; again the terms are signed, and refractive index is decreasing in both regions of the compressed window. This counterintuitive point must be emphasized: even though the window is compressing in z (geometric thickness decreasing), tensile stress in x and y is the dominant effect that explains the decreasing refractive index.

Finally, gathering everything together in (A1), the change in path length experienced for the inner beam passing through the pressurized cell is $d_w = -25.59$ fm/Pa, and for the outer beam passing through the evacuated cell $d_w = -1.84$ fm/Pa. Thus, the net effect of one pass through one window is a decrease in path length $d_{w,net} = -23.8$ fm/Pa.

APPENDIX B:: FINITE-ELEMENT MODEL OF HEAT TRANSFER

Heat transfer in the MIRE apparatus is a fairly simple problem, with only one input and one output—gas expansion and radiation, respectively—and yet difficult to accurately simulate.

Energy input from gas expansion[14] can be estimated, in the case of changing pressure in a constant volume, as $\int V \cdot \mathrm{d}p$, and the total energy for pressure fill in a constant volume is just $\Delta p \cdot V$; in the MIRE cell, a 440 kPa fill is about 31 J. In practice, a finite-element package applies heat loading in watts, so we implement gas expansion as a step-load of 0.22 W applied for the first 36 s of the simulation.

The hot gas couples through the glass triple-cell by conduction, and the dominant heat transfer mechanism from the triple-cell to the surroundings is radiation. The boundary condition for three of the four sides of the triple-cell quarter-section in Fig. 8 was radiation to the surroundings. For the bottom surface of the triple-cell in close proximity to the baseplate, the model included radiative coupling between the two planar surfaces. This coupling was a feature in the software package, but enabling it proved too computationally intensive for a desktop computer. Instead, for purposes of computational simplicity, we modeled this coupling as a conductive layer, with a heat flow equal to the analytic expression $Q_{net} = A\sigma(T_1^4 - T_2^4)/(2/\epsilon - 1)$ for two planar surfaces of area A and of the same emissivity $\epsilon = 0.85$ (glass) at temperatures T_1 and T_2, with σ being the Stefan–Boltzmann constant. This load was applied as an exponential function in time, where the function came

from a fit to the T_1 temperature transient at the bottom surface of the triple-cell when the simulation was run without any coupling between triple-cell and baseplate. The triple-cell is also thermally coupled to the baseplate by a strip of polymer shim at each end, which sets the height of the triple-cell off the baseplate; we halved the value of thermal conductivity for the polymer to account for poor thermal contact between surfaces in vacuum.

All this is to say, the finite-element model can be instructive but it is based on approximations of boundary conditions and applied load. Additionally, the gas inlet and outlet lines, which have low thermal mass and carry hot gas, have been ignored. The model is shown in Fig. 8: T_{cell} is a point probe located inside a short thermowell inside the triple-cell, approximately where the thermocouple is placed in experiment; T_{gas} is a line average probe through the gas path; $\Delta T_{\mathrm{window}}$ is the difference between two point probes on the outer surface of the window, approximately where the beams pass through.

References

1. Moldover MR, J. Res. Natl. Inst. Stand. Technol 103, 167 (1998). [PubMed: 28009367]
2. Pendrill LR, Metrologia 41, S40 (2004).
3. Heydemann PLM, Tilford CR, and Hyland RW, J. Vac. Sci. Technol 14, 597 (1977).
4. Tilford CR, Metrologia 30, 545 (1994).
5. Stone JA and Stejskal A, Metrologia 41, 189 (2004).
6. Schmidt JW, Gavioso RM, May EF, and Moldover MR, Phys. Rev. Lett 98, 254504 (2007). [PubMed: 17678030]
7. Gaiser C, Fellmuth B, Haft N, Kuhn A, Thiele-Krivoi B, Zandt T, Fischer J, Jusko O, and Sabuga W, Metrologia 54, 280 (2017).
8. Puchalski M, Piszczatowski K, Komasa J, Jeziorski B, and Szalewicz K, Phys. Rev. A At. Mol. Opt. Phys 93, 032515 (2016).
9. Egan PF, Stone JA, Ricker JE, Hendricks JH, and Strouse GF, Opt. Lett 42, 2944 (2017). [PubMed: 28957215]
10. Andersson M, Eliasson L, and Pendrill LR, Appl. Opt 26, 4835 (1987). [PubMed: 20523456]
11. Egan PF, Stone JA, Hendricks JH, Ricker JE, Scace GE, and Strouse GF, Opt. Lett 40, 3945 (2015). [PubMed: 26368682]
12. Egan PF, Stone JA, Ricker JE, and Hendricks JH, Rev. Sci. Instrum 87, 053113 (2016). [PubMed: 27250398]
13. Hall JL, Ye J, and Ma L-S, Phys. Rev. A At. Mol. Opt. Phys 62, 013815 (2000).
14. Baker B, Am. J. Phys 67, 712 (1999).
15. Scherschligt J et al., J. Vac. Sci. Technol. A 36, 040801 (2018).
16. Quinn TJ, Metrologia 34, 61 (1997).
17. Jousten K et al., Metrologia 54, S146 (2017).
18. Mohr PJ, Newell DB, Taylor BN, and Tiesinga E, Metrologia 55, 125 (2018).
19. Cencek W, Przybytek M, Komasa J, Mehl JB, Jeziorski B, and Szalewicz K, J. Chem. Phys 136, 224303 (2012). [PubMed: 22713043]
20. Garberoglio G, Moldover MR, and Harvey AH, J. Res. Natl. Inst. Stand. Technol 116, 729 (2011). [PubMed: 26989595]
21. Moldover MR and McLinden MO, J. Chem. Thermodyn 42, 1193 (2010).
22. McLinden MO, Meas. Sci. Technol 17, 2597 (2006).
23. Rourke PMC, Gaiser C, Gao B, Moldover MR, Pitre L, Madonna Ripa D, and Underwood RJ, “Refractive-index gas thermometry,” Metrologia (published online).
24. See the supplementary material at E-JVTAD6–37-321903JVA for the measured data. The supplementary material is a workbook, which contains six sheets; each sheet is labeled by the

chemical symbol for the specific candidate gas. Each sheet lists the measured n − 1, p, and T data for the specific gas in three columns. The impurity concentrations for a specific gas are given as header information in each sheet.

25. Achtermann HJ, Magnus G, and Bose TK, J. Chem. Phys 94, 5669 (1991).
26. Achtermann HJ, Hong JG, Magnus G, Aziz RA, and Slaman MJ, J. Chem. Phys 98, 2308 (1993).
27. Hohm U, Mol. Phys 81, 157 (1994).
28. McLinden MO and Lösch-Will C, J. Chem. Thermodyn 39, 507 (2007).
29. Avdiaj S, Yang Y, Jousten K, and Rubin T, J. Chem. Phys 148, 116101 (2018). [PubMed: 29566506]
30. Klopper W, Coriani S, Helgaker T, and Jørgensen P, J. Phys. B At. Mol. Opt. Phys 37, 3753 (2004).
31. Gaiser C and Fellmuth B, Phys. Rev. Lett 120, 123203 (2018). [PubMed: 29694093]
32. Polyansky OL, Bielska K, Ghysels M, Lodi L, Zobov NF, Hodges JT, and Tennyson J, Phys. Rev. Lett 114, 243001 (2015). [PubMed: 26196972]
33. Stone JA, Decker JE, Gill P, Juncar P, Lewis A, Rovera GD, and Viliesid M, Metrologia 46, 11 (2009).
34. Egan P and Stone J, 2018 Conference on Precision Electromagnetic Measurements (CPEM 2018), Paris, France (IEEE, Washington, 2018), pp. 1–2.
35. Buckley TJ, Hamelin J, and Moldover MR, Rev. Sci. Instrum 71, 2914 (2000).
36. Schmidt JW and Moldover MR, Int. J. Thermophys 24, 375 (2003).
37. Fischer J et al., Int. J. Thermophys 32, 12 (2011).
38. Boggs PT, Byrd RH, Rogers JE, and Schnabel RB, User's reference guide for ODRPACK version 2.01 software for weighted orthogonal distance regression, Technical Report NISTIR 4834, National Institute of Standards and Technology, 1992.
39. Lemmon EW, Bell IH, Huber ML, and McLinden MO, NIST Standard Reference Database 23: Reference Fluid Thermodynamic and Transport Properties—REFPROP, Version 10.0, National Institute of Standards and Technology, 2018.
40. Span R and Wagner W, J. Phys. Chem. Ref. Data 25, 1509 (1996).
41. Tegeler C, Span R, and Wagner W, J. Phys. Chem. Ref. Data 28, 779 (1999).
42. Span R, Lemmon EW, Jacobsen RT, Wagner W, and Yokozeki A, J. Phys. Chem. Ref. Data 29, 1361 (2000).
43. Lemmon EW and Span R, J. Chem. Eng. Data 51, 785 (2006).
44. Thol M, Beckmüller R, Weiss R, Harvey AH, Lemmon EW, Jacobsen RT, and Span R, "Thermodynamic properties for neon for temperatures from the triple point to 700 K at pressures to 700 MPa," J. Phys. Chem. Ref. Data (unpublished).
45. Burns R, Graham C, and Weller A, Mol. Phys 59, 41 (1986).
46. Hohm U and Kerl K, Mol. Phys 69, 803 (1990).
47. Birch KP, J. Opt. Soc. Am. A Opt. Image Sci. Vis 8, 647 (1991).
48. Coulon R, Montixi G, and Occelli R, Can. J. Phys 59, 1555 (1981).
49. Hou W and Thalmann R, Measurement 13, 307 (1994).
50. Egan PF and Stone JA, Appl. Opt 50, 3076 (2011). [PubMed: 21743505]
51. Hohm U and Trümper U, Mol. Phys 89, 943 (1996).
52. Montixi G, Coulon R, and Occelli R, Can. J. Phys 61, 473 (1983).
53. Achtermann HJ, Bose TK, Rögener H, and St-Arnaud JM, Int. J. Thermophys 7, 709 (1986).
54. May EF, Moldover MR, and Schmidt JW, Phys. Rev. A At. Mol. Opt. Phys 78, 032522 (2008).
55. May EF, Moldover MR, and Schmidt JW, Mol. Phys 107, 1577 (2009).
56. Kumar A and Thakkar AJ, J. Chem. Phys 132, 074301 (2010). [PubMed: 20170221]
57. Barter C, Meisenheimer RG, and Stevenson DP, J. Phys. Chem 64, 1312 (1960).
58. Pendrill LR, Phys J. B At. Mol. Opt. Phys 29, 3581 (1996).
59. Shelton DP, Rev. Sci. Instrum 63, 3978 (1992).
60. Bartl G, Glaw S, Schmaljohann F, and Schödel R, Metrologia 56, 015001 (2019), and corrigendum, in preparation.

61. Harvey AH and Lemmon EW, Int. J. Thermophys 26, 31 (2005).
62. Buldakov MA, Matrosov II, and Cherepanov VN, Opt. Spectrosc 89, 37 (2000).
63. Sharipov AS, Loukhovitski BI, and Starik AM, J. Phys. B At. Mol. Opt. Phys 49, 125103 (2016).
64. Guenther BD, Modern Optics, 2nd ed. (Oxford University, New York, 2015).
65. Borrelli NF and Miller RA, Appl. Opt 7, 745 (1968). [PubMed: 20068676]
66. Schott Glass: TIE-27: Stress in optical glass, Technical Report (Schott AG, 2004).

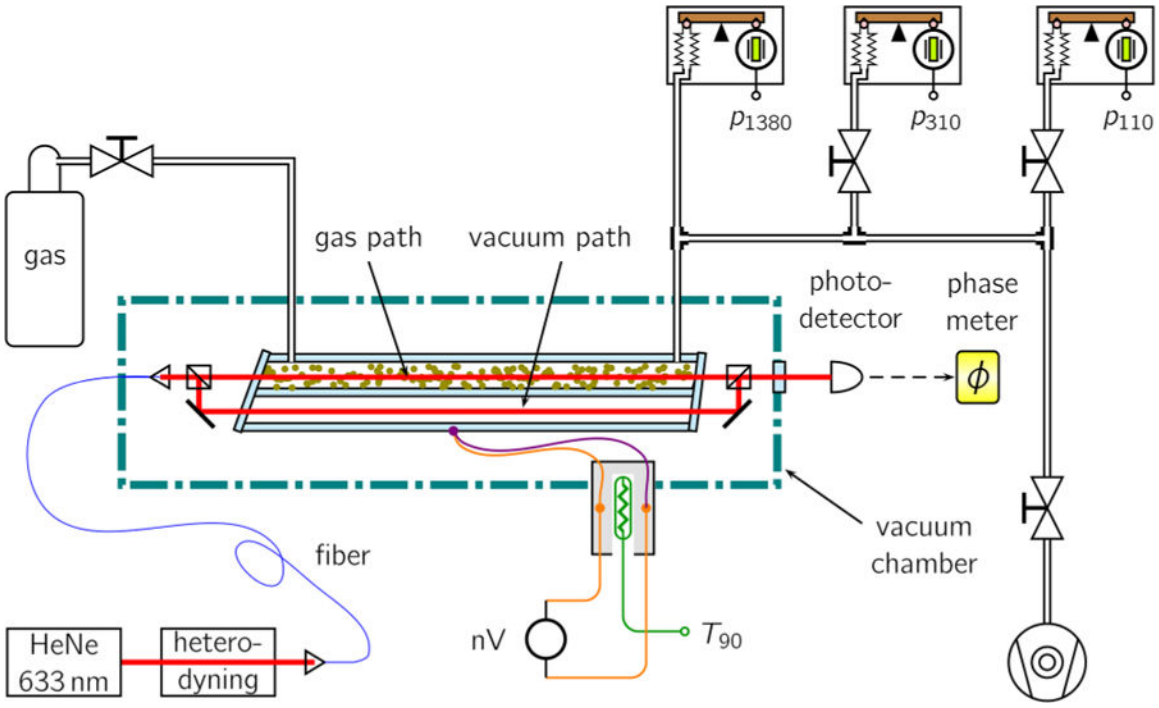

FIG. 1.

Schematic of the gas metrology system. Optical layout is illustrative and does not show the actual quadpass interferometer and triple-cell scheme.

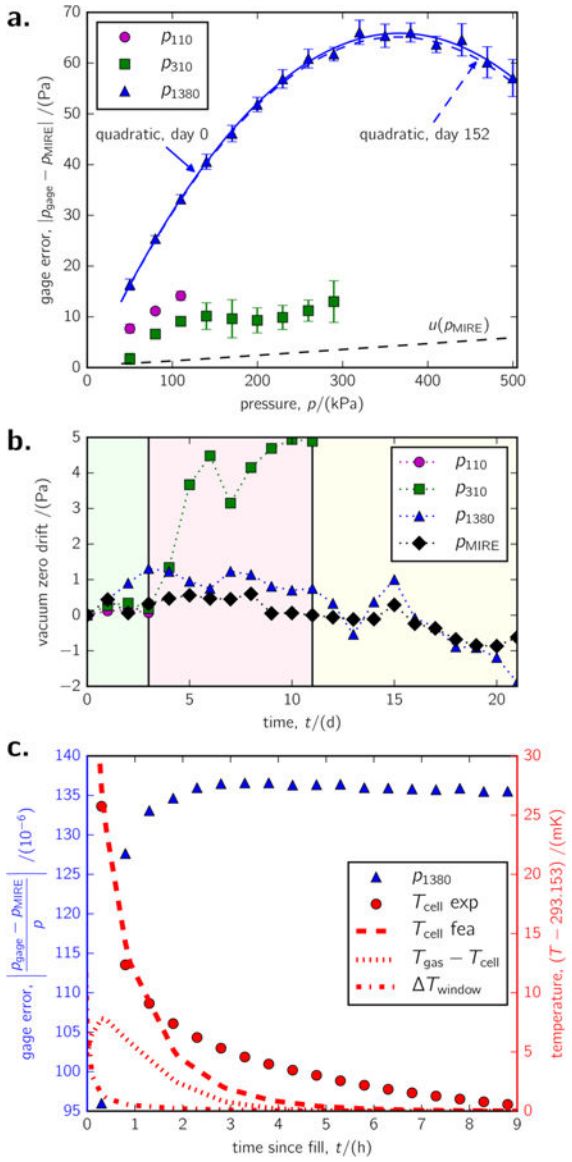

FIG. 2.

(a) Calibration data for the three pressure gages obtained by measurement of helium refractivity at a known temperature in MIRE. (b) Drift in the three gages when at vacuum during the three weeks of calibration. (c) Gas pressure error and temperature readings over time immediately after a 440 kPa helium fill. The dashed lines come from a finite-element model of heat transfer.

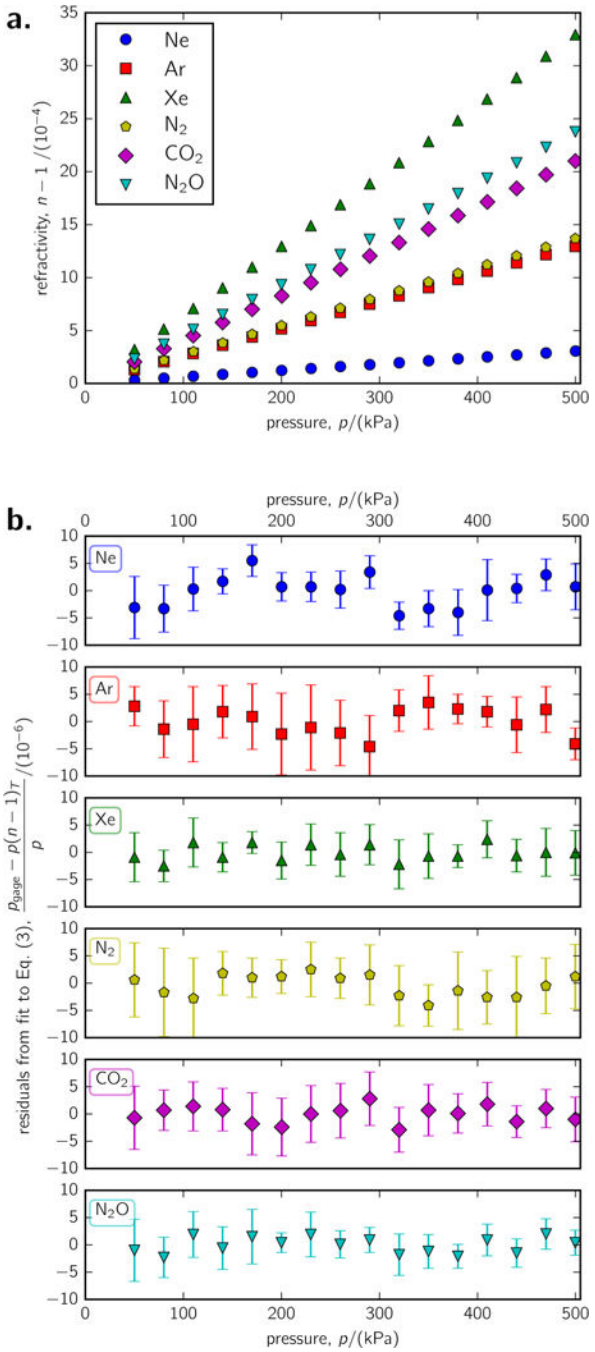

FIG. 3.

(a) Measurements of refractivity as a function of pressure for each gas. (b) Residuals on the regression for each of the six gases measured. The pressure reading p_{gage} comes from the calibrated pressure gages; fit pressure $p(n-1)_T$ comes from measurements of gas refractivity using (3) with the proportionality coefficients of Table I. The error bars span $\pm\sigma$, the standard deviation on the sample of ten repeat measurements at each pressure point.

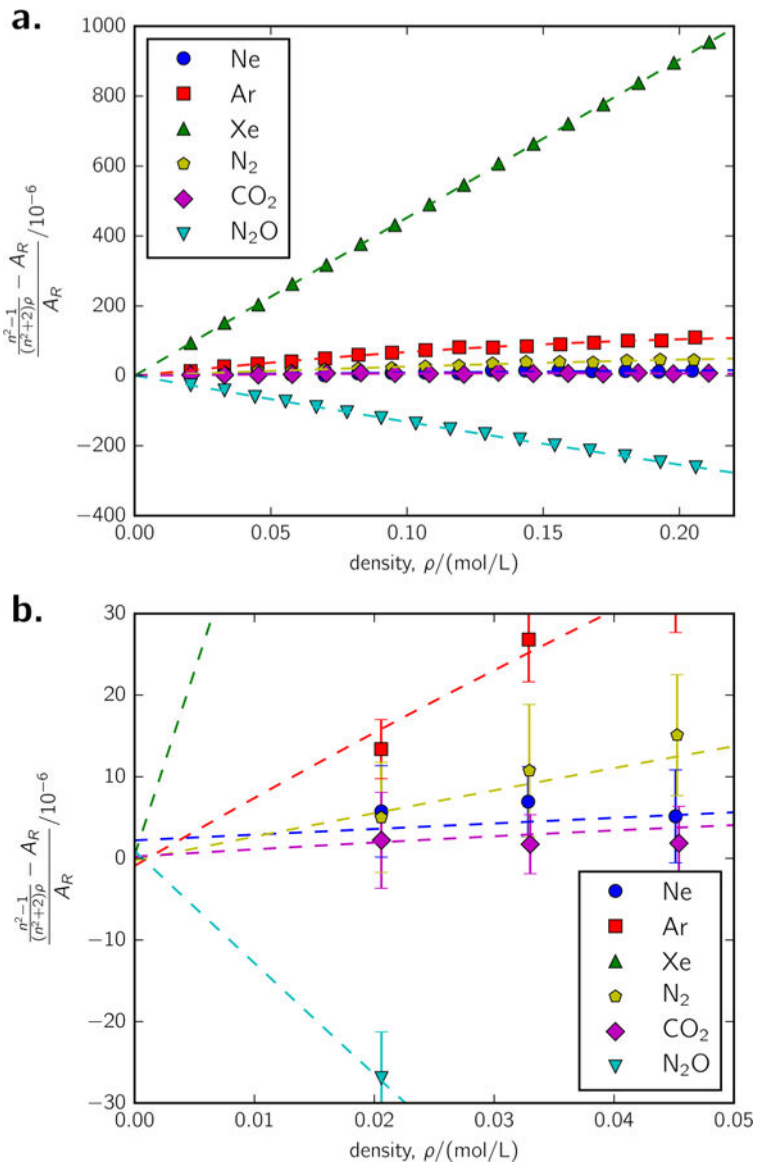

FIG. 4.

(a) Measured data analyzed in terms of the Lorentz–Lorenz quotient and with density calculated from reference equations of state. (b) Zoom on the *y*-axis intercept.

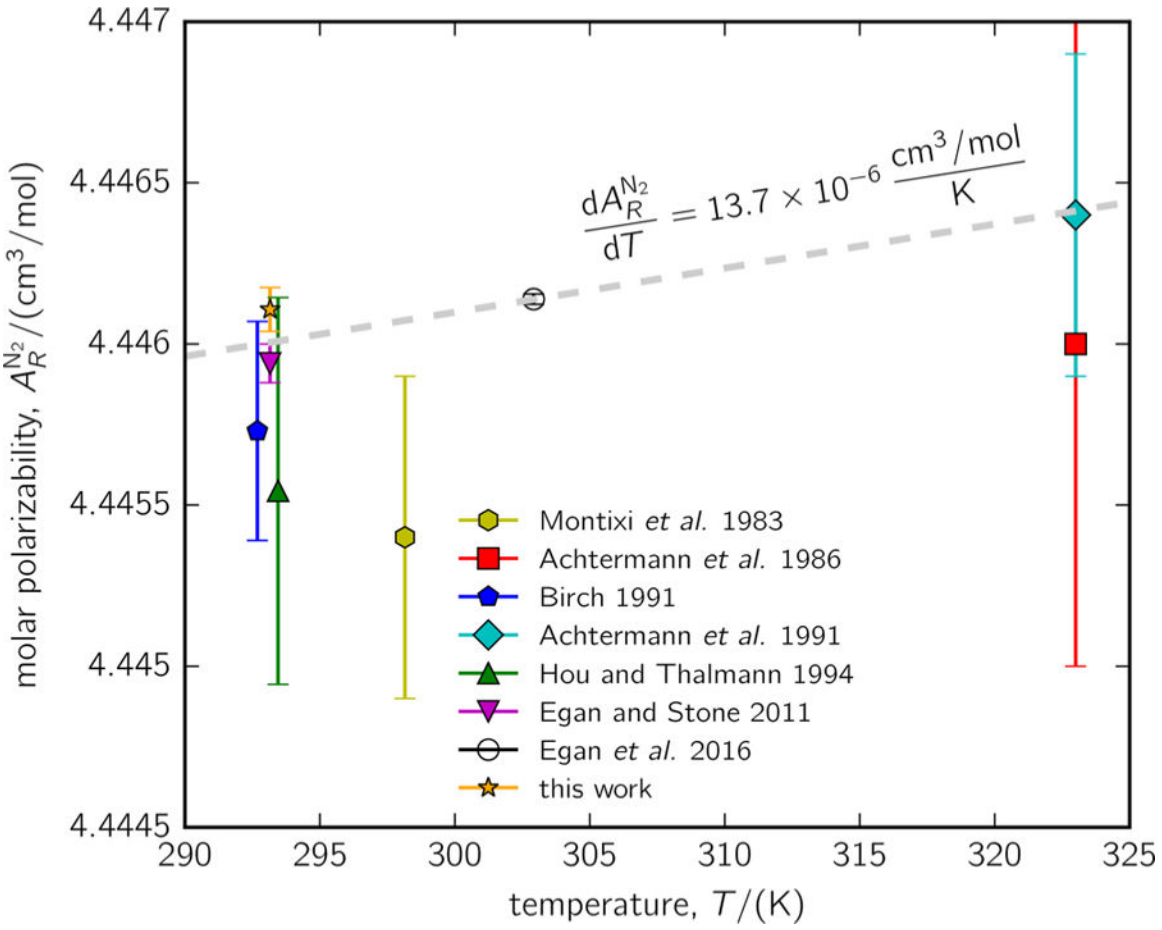

FIG. 5.

Literature measurements of the molar polarizability of nitrogen as a function of temperature. The error bars span standard uncertainties.

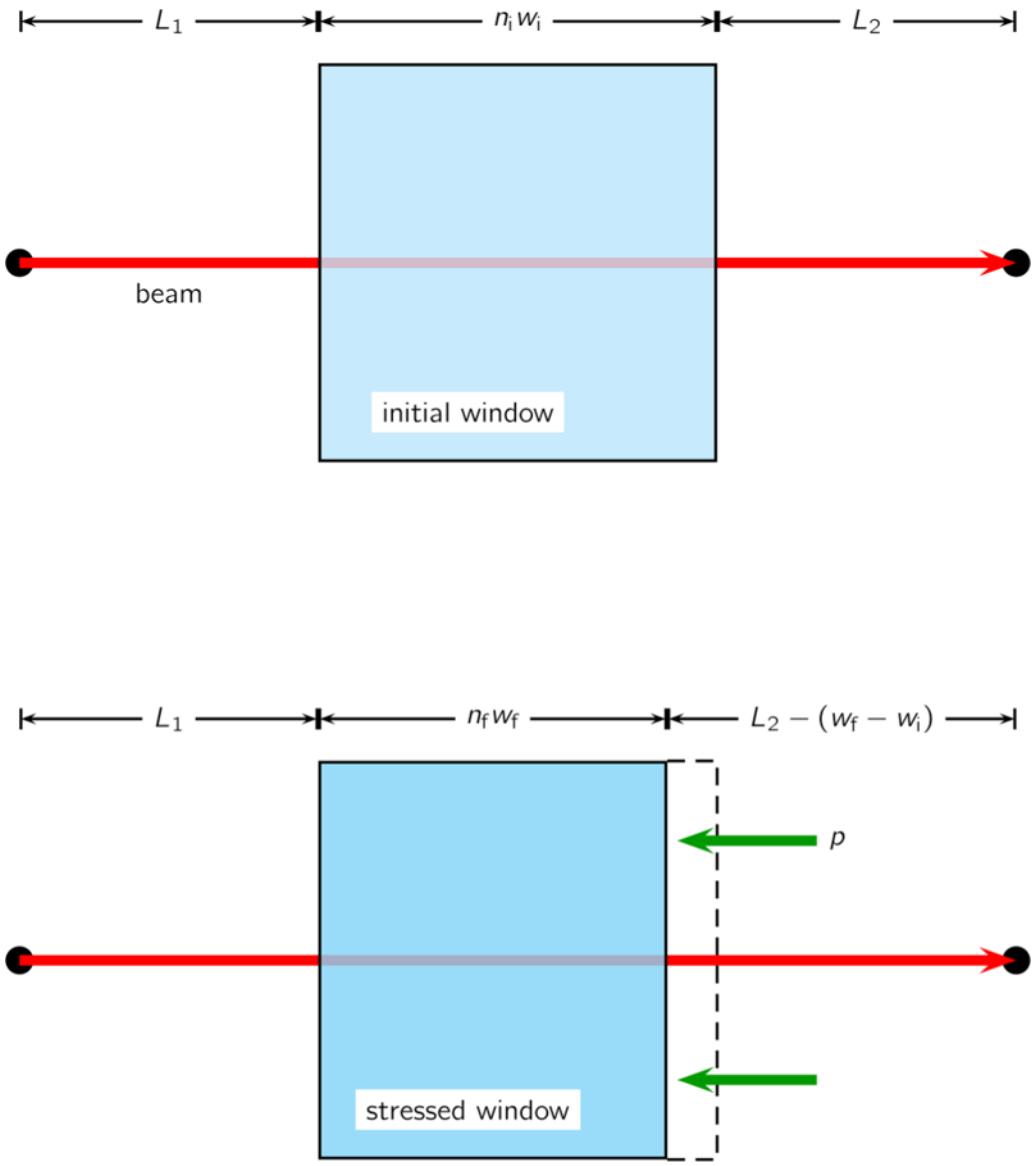

FIG. 6.

Change in path length through a window that becomes distorted by applied pressure p is measured between two external fixed points,

$d_w \cdot p = [L_1 + n_f w_f + L_2 - (w_f - w_i)] - (L_1 + n_i w_i + L_2)$.

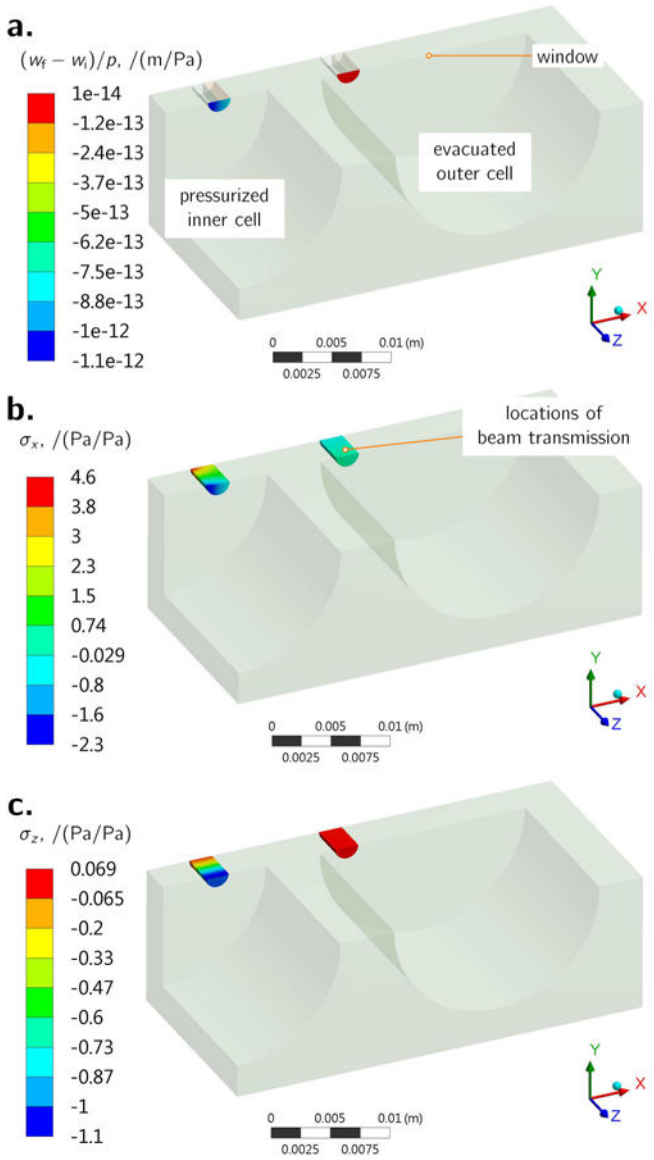

FIG. 7.

(a) Geometric thinning at the window surfaces. (b) and (c) Normal stress in the *x*- and *z*-axes through the window. Stress in the *y*-axis (not shown) is similar to that of the *x*-axis. In each of these cases, 1 Pa has been applied to the (inner) pressurized cell.

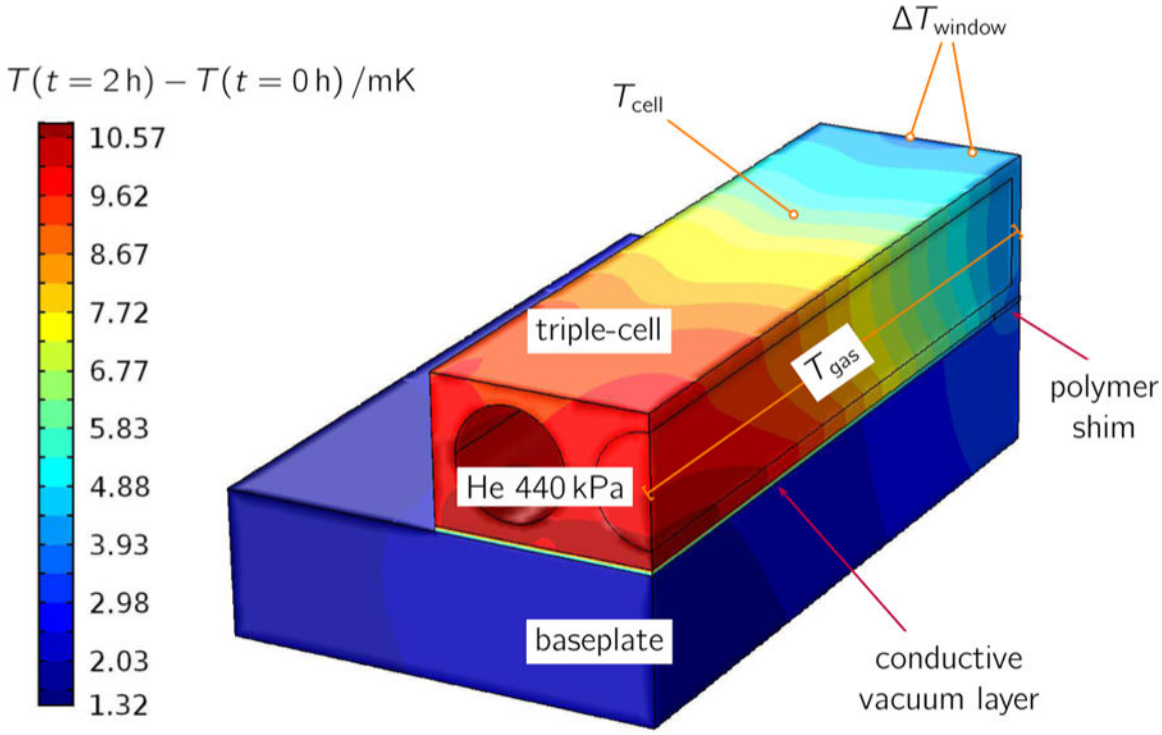

FIG. 8.

Finite-element model of transient heat transfer in the MIRE apparatus, on one side of the symmetry axes (i.e., a quarter-section). The figure shows the temperature distribution throughout the triple-cell and baseplate 2 h after the center cell has been filled to 440 kPa helium.

TABLE I.

Proportionality coefficients of Eq. (3) for the gases measured at $T = 293.1529(13)$ K and $\lambda = 632.9908(2)$ nm. The numbers in brackets are the statistical uncertainties of the weighted orthogonal distance regression only.

Gas	$c_1 \times 10^{-8}$ (Pa)	$c_2 \times 10^{-8}$ (Pa)	$c_3 \times 10^{-10}$ (Pa)
Ne	16.245968(29)	119.84(36)	32.5(98)
Ar	3.8728820(80)	−11.371(25)	2.66(17)
Xe	1.5638229(21)	−14.0785(26)	0.4956(67)
N_2	3.6547460(79)	−4.005(23)	1.47(15)
CO_2	2.4459350(40)	−31.8197(76)	−1.372(31)
N_2O	2.1668132(27)	−26.7190(45)	0.920(16)

TABLE II.

Relative standard uncertainty in our determination of molar polarizability A_R for each candidate gas.

	$u(A_R) \times 10^6$					
Component	**Ne**	**Ar**	**Xe**	**N_2**	**CO_2**	**N_2O**
p	14.2	14.2	14.5	14.2	14.3	14.3
T	4.5	4.5	4.5	4.5	4.5	4.5
$n-1$	5.2	1.3	0.5	1.2	0.8	0.7
Impurity	2.5	0.1	3.0	0.1	0.2	0.4
Regression	1.8	2.1	1.3	2.2	1.6	1.2
Combined	16.0	15.1	15.5	15.1	15.1	15.3

TABLE III.

Comparison of our work with the literature for molar polarizabilities measured at 633 nm. Our A_R is deduced from $c_1 = \frac{2RT}{3A_R}$, with $R = k_B \cdot N_A$ using $k_B = 1.380649 \times 10^{-23}$ J/K and $N_A = 6.0221408 \times 10^{23}$ mol^{-1} from CODATA (Ref. 18). The numbers in brackets express standard uncertainties.

Gas	A_R (cm^3/mol)	References
Ne	0.999(1)	Burns *et al.* (Ref. 45)
	1.001(1)	Hohm and Kerl (Ref. 46)
	1.00170(8)	Birch (Ref. 47)
	1.0012(2)	Achtermann *et al.* (Ref. 26)
	1.000211(16)	This work
Ar	4.1973(5)	Coulon *et al.* (Ref. 48)
	4.1953(3)	Birch (Ref. 47)
	4.1955(3)	Achtermann *et al.* (Ref. 26)
	4.1962(7)	Hohm (Ref. 27)
	4.1955(6)	Hou and Thalmann (Ref. 49)
	4.19553(6)[a]	Egan and Stone (Ref. 50)
	4.195685(64)	This work
Xe	10.36(1)	Burns *et al.* (Ref. 45)
	10.345(2)	Achtermann *et al.* (Ref. 26)
	10.395(6)	Hohm and Trümper (Ref. 51)
	10.39081(16)	This work
N_2	4.4454(5)	Montixi *et al.* (Ref. 52)
	4.446(1)	Achtermann *et al.* (Ref. 53)
	4.4457(3)	Birch (Ref. 47)
	4.4464(5)	Achtermann *et al.* (Ref. 25)
	4.4455(6)	Hou and Thalmann (Ref. 49)
	4.44594(6)	Egan and Stone (Ref. 50)
	4.446139(16)	Egan *et al.* (Ref. 12)
	4.446107(68)	This work
CO_2	6.6418(5)	Birch (Ref. 47)
	6.644(1)	Achtermann *et al.* (Ref. 25)
	6.646(3)	Hohm (Ref. 27)
	6.64343(11)	This work
N_2O	7.5021(7)	Birch (Ref. 47)
	7.5114(6)	Hohm (Ref. 27)
	7.49921(12)	This work

[a] Adjusted by $+19.3 \times 10^{-6}$. A_R from what was reported in Ref. 50 to account for two biases; see the text for details.